Low temperature wet-chemical synthesis of spherical hydroxyapatite nanoparticles and their *in situ* cytotoxicity study

Sudip Mondal[1], Apurba Dey[2] and Umapada Pal[*1]

[1]*Instituto de Física, Universidad Autónoma de Puebla, Apdo. Postal J-48, Puebla, Pue. 72570, Mexico*
[2]*Department of Biotechnology, National Institute of Technology Durgapur,
M.G. Avenue, Durgapur-713209, Burdwan, WB, India*

Abstract. The present research work reports a low temperature (40°C) chemical precipitation technique for synthesizing hydroxyapatite (HAp) nanoparticles of spherical morphology through a simple reaction of calcium nitrate tetrahydrate and di-ammonium hydrogen phosphate at pH 11. The crystallinity of the single-phase nanoparticles could be improved by calcinating at 600°C in air. Thermogravimetric and differential thermal analysis (TG-DTA) revealed the synthesized HAp is stable up to 1200°C. Scanning electron microscopy (SEM) and energy dispersive spectroscopy (EDS) studies confirmed the formation of spherical nanoparticles with average size of 23.15±2.56 nm and Ca/P ratio of 1.70. Brunauer-Emmett-Teller (BET) isotherm of the nanoparticles revealed their porous structure with average pore size of about 24.47 nm and average surface area of 78.4 m^2g^{-1}. Fourier transform infrared spectroscopy (FTIR) was used to confirm the formation of P-O, OH, C-O chemical bonds. Cytotoxicity and MTT assay on MG63 osteogenic cell lines revealed nontoxic bioactive nature of the synthesized HAp nanoparticles.

Keywords: hydroxyapatite; nanomaterials; wet chemical precipitation; biomaterials

1. Introduction

Nowadays, calcium phosphates are the materials of choice for different pharmaceutical applications like tissue engineering, drug delivery, drug formulation, dentistry and medicine (Uskokoviƈc and Wu 2016). Calcium phosphate compounds, classified according to their chemical compositions are described in Table 1. Hydroxyapatite $[Ca_{10}(PO_4)_6(OH)_2]$ is one of the most effective inorganic calcium phosphate compound extensively studied for biomedical applications. To be a good biomaterial, it is always desirable that the material have a high degree of crystallinity and chemical stability (Tsui, Doyle *et al.* 1998). However, poor mechanical properties, such as poor hardness, low tensile and compressive strength restrict HAp for applications only to those that require little or no load-bearing functions (Liu, Troczynski *et al.* 2001). HAp has also been studied for other non-medical applications. For example, as packing material for column chromatography (Morales, Burgues *et al.* 2001), catalyst (Tanaka, Chikazawa *et al.* 2000), chemical gas sensor (Nagai, Nishino *et al.* 1988) and in fuel cells (Gross, Berndt *et al.* 1998). In

---

∗Corresponding author, Professor, E-mail: upal@ifuap.buap.mx

nanostructure form, HAp has attracted considerable attention as promising carrier material for drug delivery applications (Panda, Ming-Fa *et al.* 2001). However, the diverse applications of HAp require its material properties to be tailored accordingly. Hence, researchers have tried to customize its properties such as stoichiometry, size, morphology, mechanical strength, solubility and sinterability. The chemical, structural and morphological properties of synthetic HAp can be modulated by varying the synthesis methodology along with controlling synthesis parameters such as pH, temperature, precursor molecules etc.

Classical methods for HAp powder synthesis include chemical precipitation, sol-gel, emulsion system, hydrothermal processing, microwave route, spray pyrolysis, solid state reactions, and sonochemical synthesis (Shojai, Khorasani *et al.* 2013). Liu, Yang *et al.* (2002) have synthesized HAp nanoparticles (nano-HAp) of 8-10 nm sizes via template mediated and non-template mediated sol-gel techniques. Varma, Kalkura *et al.* (1998) synthesized nano-HAp by polymeric combustion and self-propagating combustion methods using novel body fluid solutions. Shih *et al.* (2004) synthesized nano-HAp powder (Ca/P=1.67) of 20 nm particle size through hydrolysis. An annealing temperature of 1000°C resulted in an average increase in particle diameter to 50 nm after heat soaking for 4 h. Nasiri-Tabrizi, Honarmandi *et al.* (2009) synthesized single-crystal HAp nanorods and nanogranules through mechanochemical process in polyamide 6 milling medium. Xu, Khor *et al.* (2004) used radio frequency plasma spray process to synthesize nano-sized HAp powder with particle size in the range of 10-100 nm. Kuriakose, Kalkura *et al.* (2004) synthesized nanocrystalline HAp of about 1.3 nm radius, which are stable up to 1200°C without any by-products, using ethanol as a solvent. Synthesis of pure HAp crystals of 8-10 nm size is reported by a novel sol-gel technique using agar (Kuriakose, Kalkura *et al.* 2004). Han, Wang *et al.* (2004) synthesized HAp nanoparticles at relatively low temperature (750°C) by citric acid sol-gel combustion method. Adhikary, Takahashi *et al.* (2004) have also synthesized HAp nanoparticles through sol-gel combustion process using citric acid, obtaining particles between 80 and 150 nm and porosity of about 19%. On the other hand, Sarig and Kahana (2002) could fabricate plate-shaped nanoparticles of HAp through direct precipitation from dilute calcium chloride and sodium phosphate solutions by microwave irradiation. The pH of the mixture solution was kept at 7.4 to fabricated HAp particles suitable for medical applications.

Wet chemical process based on chemical precipitation is the most convenient and commonly used process for HAp fabrication. This process is very simple and easy to use, offering a molecular level mixing of calcium and phosphorus precursors to improve the chemical homogeneity of the product, apart from reducing synthesis temperature. The precipitation technique has been developed and used to synthesize nanomaterials with different Ca/P ratios by altering the quantity and the composition of precursors and processing variables. The powders synthesized by precipitation method are frequently calcinated in between 400 and 600°C or even at higher temperature in order to obtain stoichiometric apatitic structures. In some cases, a well-crystallized HAp phase develops only after calcinating as-prepared samples around 1200°C (Mondal, Mahata *et al.* 2010). However, the composition, physicochemical properties, crystal size and morphology of synthetic apatites are extremely sensitive to preparation conditions. Frequently, non-stoichimetric calcium deficient HAp powders are produced. Raynaud, Champion *et al.* (2002) synthesized single-phase calcium phosphate powders with Ca/P molar ratio ranging from 1.5 to 1.67, using wet chemical methods. Temperature and pH of the reaction solution were found to be important parameters for controlling the composition of the precipitates. Slow titration process and use of diluted precursor solution are seen to improve the chemical homogeneity, morphology and stoichiometry of HAp synthesized by chemical precipitation. Therefore, careful control of reaction

Table 1 Calcium phosphate compounds: Ca/P molar ratio, chemical formula, and acronym (Kehoe 2008)

Calcium Phosphate	Ca/P molar ratio	Chemical Formula	Acronym
Tetracalcium phosphate	2.0	$Ca_4O(PO_4)_2$	TTCP
Hydroxyapatite	1.67	$Ca_{10}(PO_4)_6(OH)_2$	HA, HAp, HAP
Oxyapatite	1.67	$Ca_{10}(PO_4)_6O$	OXA
Calcium deficient hydroxyapatite	1.33 - 1.67	$Ca_{10-x}H_x(PO_4)_6(OH)_{2-x}$	*Ca-d*HAp
α - Tricalcium phosphate	1.5	α - $Ca_3(PO_4)_2$	α - TCP
β - Tricalcium phosphate	1.5	β - $Ca_3(PO_4)_2$	β - TCP
γ - Tricalcium phosphate	1.5	γ - $Ca_3(PO_4)_2$	γ - TCP
Octacalcium phosphate	1.33	$Ca_4H(PO_4)_3.3H_2O$	OCP
Dicalcium phosphate anyhdrous	1.00	$CaHPO_4$	DCPA
Dicalcium phosphate dihydrate	1.00	$CaHPO_4 \cdot 2H_2O$	DCPD
Calcium pyrophosphate (α, β, γ)	1.00	α - $Ca_2P_2O_7$ β - $Ca_2P_2O_7$ γ - $Ca_2P_2O_7$	α -CPP β -CPP γ -CPP
Calcium pyrophosphate dihydrate	1.00	$Ca_2P_2O_7 \cdot 2H_2O$	CPPD
Heptacalcium phosphate	0.7	$Ca_7(P_5O_{16})_2$	HCP
Tetracalcium dihydrogen phosphate	0.65	$Ca_4H_2P_6O_{20}$	TDHP
Monocalcium hydrate monohydrate	0.5	$Ca(H_2PO_4)_2 \cdot H_2O$	MCPM
Calcium metaphophate (α, β, γ)	0.5	$Ca(PO_3)_2$	CMP
Amorphous calcium phosphate		$Ca_3(PO_4)_2 \cdot 3H_2O$	ACP

conditions is critical in wet precipitation process. A decrease of solution pH below 9.0 could lead to the formation of Ca-deficient HAp structures (Liu, Yang *et al.* 2001). Most of the wet chemical methods are time-consuming as the formation of HAp phase and rinsing of excess anions from their surface take time. In this work, we synthesized nanocrystalline HAp powder using stoichiometric amount of calcium nitrate and di-ammonium hydrogen phosphate at a low temperature (40℃).

2. Materials and methods

2.1 Chemicals and reagents

Calcium nitrate tetrahydrate [$Ca(NO_3)_2 \cdot 4H_2O$, 99%, CAS: 13477-34-4], di-ammonium hydrogen phosphate [$(NH_4)_2HPO_4$, 98%, CAS:7783-28-0], and ammonium hydroxide [NH_4OH, 28%, CAS: 1336-21-6] were procured from Sigma Aldrich, Mexico. Ethanol [C_2H_5OH, CTR 01160] was purchased from CTR scientific chemicals, Mexico. During synthesis, deionized water (ρ>18.2 Ω.cm) from a Millipore system was used as solvent.

2.2 Experimental procedure

HAp powder was synthesized by solution-precipitation method, using calcium nitrate
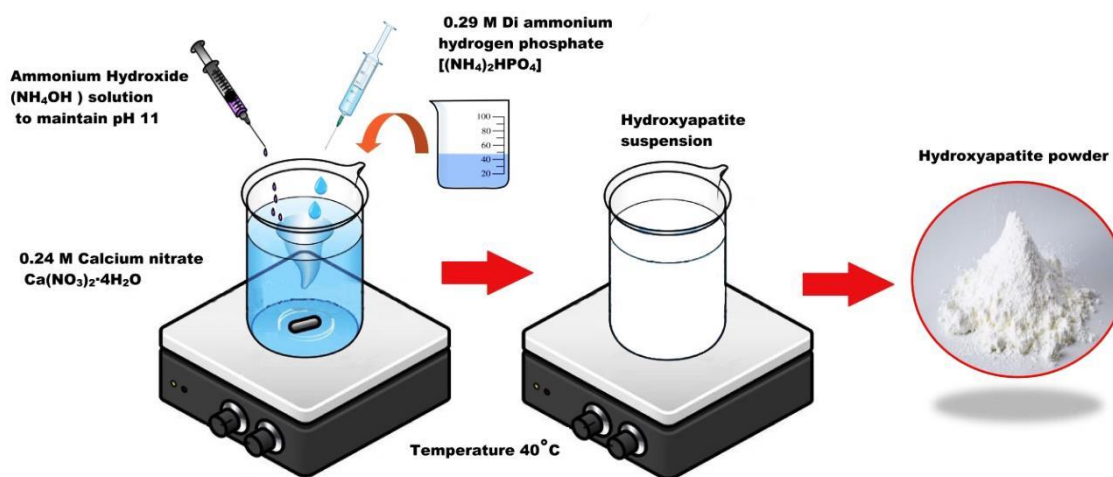
Fig. 1 Schematic presentation of the chemical precipitation process used to synthesize HAp nanoparticles

tetrahydrate [$Ca(NO_3)_2 \cdot 4H_2O$, Sigma Aldrich] and di-ammonium hydrogen phosphate [$(NH_4)_2HPO_4$, Sigma Aldrich] as starting materials and ammonia (NH_4OH) solution as precipitating agent (Mobasherpour, Soulati Heshajin *et al.* 2007). A suspension of 0.24 M $Ca(NO_3)_2 \cdot 4H_2O$ (23.61 g $Ca(NO_3)_2 \cdot 4H_2O$ in 350 mL deionized water) was vigorously stirred, maintaining its temperature at 40°C. Then a solution of 0.29 M $(NH_4)_2HPO_4$ (7.92 g $(NH_4)_2HPO_4$ in 250 mL deionized water) was added dropwise to the $Ca(NO_3)_2 \cdot 4H_2O$ solution (Fig. 1). The pH of the final mixture was adjusted to 11 by drop-wise addition of ammonia solution. The reaction occurred could be expressed as:

$$10Ca(NO_3)_2 \cdot 4H_2O + 6(NH_4)_2HPO_4 + 8NH_4OH \rightarrow Ca_{10}(PO_4)_6(OH)_2 + 20NH_4NO_3 + 20H_2O \quad (1).$$
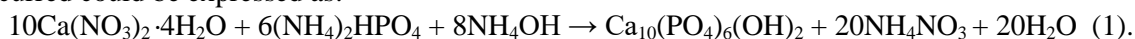
After 1 h of reaction followed by 24 h of ageing, the formed precipitate was removed from the reaction solution by centrifugation at 5000 rpm for 6 minutes and dried at 80°C for 1 h. The dry powder was calcinated at 600°C for 1 h in air.

2.3 Characterization of hydroxyapatite

2.3.1 X-ray diffraction (XRD)

The structural characterization of the resulting powder after calcination was carried out by powder X-ray diffraction analysis (30 KeV and 25 mA) using Cu Kα radiation (λ=1.5406 Å) of a Bruker 8D diffractometer. The XRD spectrum of the sample was compared with standard diffraction data (JCPDS# 72-1243) of pure HAp, wherein the estimated *d* values were found to be in good agreement with the standard data.

2.3.2 Fourier transformed infrared spectroscopy (FTIR)

To determine the functional groups present in HAp powder, its FTIR spectrum was recorded in a Perkin Elmer Spotlight 400 FT-IR instrument in the scanning range of 4000-400 cm^{-1} using a cold pressed pellet of potassium bromide (KBr, Merck) containing 1% HAp sample.

2.3.3 Brunauer-Emmett-Teller (BET) analysis

The BET-average pore size, pore volume and surface area of the synthesized HAp powder were estimated from the nitrogen physisorption isotherm of the sample measured at 77 K, using a BEL SORP- mini-II (Japan) instrument. Before recording the nitrogen adsorption-desorption isotherm, the sample was degassed under vacuum at 250℃ for 6 h.

2.3.4 Thermogravimetric and differential thermal analysis (TG-DTA)

TG measures mass changes in a material as a function of temperature (or time) under a controlled atmosphere. TG-DTA analysis of the synthesized HAp was carried out in a NETZSCH Jupiter TG-DTA instrument in nitrogen atmosphere in the 25-1200℃ temperature range, at a heating rate of 10℃/ min.

2.3.5 Scanning electron microscopy (SEM) and Energy dispersive spectroscopy (EDS)

The morphology and chemical composition of the HAp powder were studied by a field-emission scanning electron microscope (FE-SEM, SUPRA 40, CARLZEISSSMT, Oxford) coupled with Oxford analytical system, operating at 25 KeV. For this analysis, the powder sample was dispersed in ethanol and spread over either a carbon tape or silicon wafer and dried at room temperature.

2.3.6 Biocompatibility and toxicity tests

Experimental study from different researchers concluded that HAp continues to show an extremely attractive biogenic profile. This profile includes low toxicity, lack of inflammatory or immunogenic foreign-body response to the material in solid or particulate form, a lack of pyrogenic response, absence of intervening fibrous tissue between implant and bone, and the affinity to be bonded to bone directly. The synthesized HAp powder was screened *in vitro* for cytotoxic effects on cultured MG63 cells. Cytotoxicity effects were analysed by Trypan blue staining and MTT assay.

2.3.7 Trypan blue staining

Trypan blue stain is a dye exclusion technique for viable cell counting. This method is based on the principle that live (viable) cells do not uptake certain dyes, whereas dead (non-viable) cells retain the dye. The synthesized HAp powder was steam sterilized in an autoclave chamber. Under these conditions, steam at a pressure of 15 pounds per square inch (psi), attaining temperature (121℃) killed all organisms and their endospores in about 15 minutes. The sterilized autoclaved powder tested for *in vitro* cytotoxicity in MG63 cell lines. In a 24 well cell cultured plate, MG63 osteogenic cells were cultured (10^5 cells/cm^2) in Dulbecco's Modified Eagle Medium (DMEM) containing 10% Fetal bovine serum (FBS) with a total volume of 500 μL of cell culture suspensions. For synthesized HAp nanoparticles cytotoxicity test, 50 μg of sterilized HAp nanoparticles were introduced into the culture well. The control plate for this cytotoxicity study contained only MG63 cell lines (without any HAp nanoparticles). After 24 h of incubation in 5% CO_2 incubator at 37℃ temperature, the cells were stained with trypan blue (1:1 dilution of the cell suspension using a 0.4% Trypan blue solution) and carefully fill the hemocytometer chamber. After incubation of the cells for 1- 2 minutes at room temperature, the cultured plate was observed under inverted microscope for viable cell count (Mondal, Mondal *et al.* 2014).

2.3.8 MTT assay

This colorimetric assay measures the reduction of yellow 3-(4, 5-dimethythiazol- 2-yl)-2, 5-diphenyl tetrazolium bromide (MTT) by mitochondrial succinate dehydrogenase. The MTT enters the cells and passes into the mitochondria where it is reduced to an insoluble, coloured (dark purple) formazan product (Stockert, Castro *et al.* 2012). Since the reduction of MTT can only occur in metabolically active cells, the measurement of formazan represents the viability of the cells. To perform the MTT [(3-(4,5-dimethylthiazol-2-yl)-2,5-diphenyltetrazolium-bromide)] assay, MG63 cell lines were seeded in 96 multi well plates, at 10^4 cell/cm^2 density in $100\mu L$ of growth medium. After 24 h, the cells were exposed to the synthesized HAp at a final concentration of $100\mu g/mL$ for a period of 24, 48 and 72 h at 37°C with 5% CO_2. The control well does not contain any HAp particle in this MTT assay study. After each incubation time, the cells were incubated with $10\mu L$ of a 0.5mg/mL MTT solution, for 4 h in the incubator. By the end of this period, the medium as removed and the produced formazan crystals were dissolved in $100\mu L$ dimethyl sulfoxide (DMSO).

The concentration of the coloured formazan was measured at 570 nm in a scanning multi-detection spectrophotometer micro plate reader (Biorad, USA). All the experiments were performed in triplicate. Cytotoxicity can expressed as a percentage of cell viability considering 100% viability in the control (cells treated with 1% DMSO in culture medium):

$$\text{The percentage of cell viablility } = \frac{\text{Absorbance of treated cells}}{\text{Absorbance of controlled cells}} \text{ X } 100\text{ \%}$$

3. Results and discussion

3.1 XRD

Fig. 2(a) presents the XRD pattern of the calcinated HAp sample. Appearance of sharp well-defined peaks in the diffraction pattern indicates its high crystallinity. Well-resolved characteristic peak of highest intensity obtained at 2θ=31.77° corresponds to the (211) plane of HAp (JCPDS#72-1243). Presence of this characteristic HAp peak, along with other peaks around 31°, 33°, 38.5°, 45°, 48°, 52° confirms the formation of stoichiometric HAp in apatite phase. According to the literature, the calcium carbonate peak appears at 39.9°. However, it is very difficult to assign this peak to impurity because of overlapping of carbonate and HAp planes. All the diffraction peaks matched well with the standard diffraction data of apatite HAp and with that reported in the literature (Vaidhyanathan and Rao 1996).

3.2 FTIR

The FTIR absorption spectrum of the HAp sample synthesized by wet chemical process is shown in Fig. 2(b). The spectrum revealed characteristic bands of PO_4^{3-} at around 472, 575, 601, 963, 1059, and 1100 cm^{-1}. The absorption band appeared at 472 cm^{-1} is attributed to the $v2$ bending vibration. The band appeared around 963 cm^{-1} corresponds to $v1$ and the bands appeared in between 1059 and 1100 cm^{-1} correspond to the $v3$ vibrations of PO_4^{3-} ions (Mondal *et al.* 2010). The absorption bands appeared at 575 cm^{-1} (Jillavenkatesa, Hoelzer *et al.* 1999) and 601 cm^{-1} can be attributed to the n4 fundamental bending mode of (PO_4^{3-}) functional group (Rivera, Araiza *et al.*
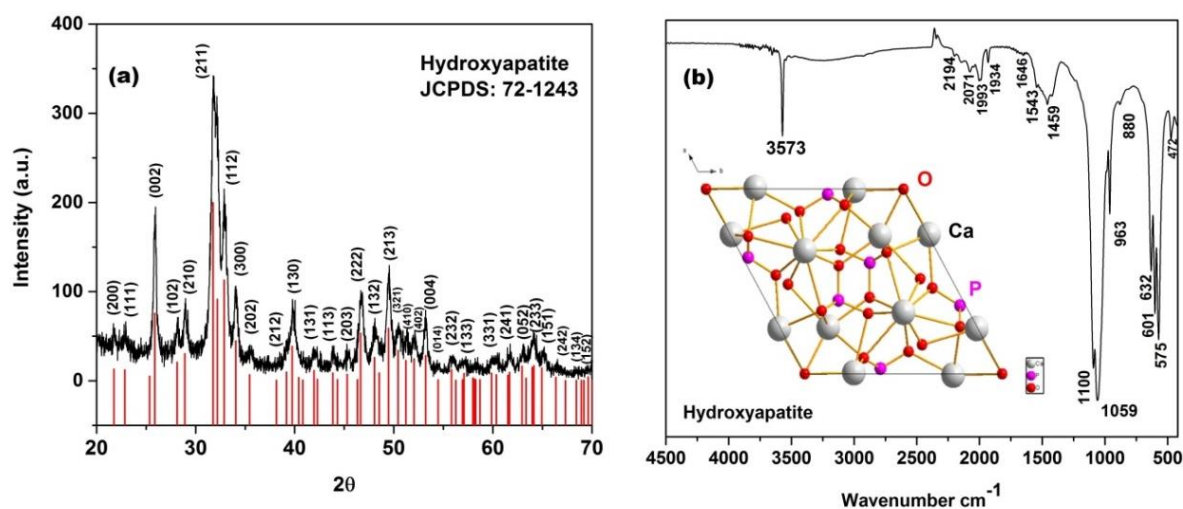
Fig. 2 (a) XRD and (b) FTIR spectra of calcinated HAp nanoparticles

1999); while the bands appeared in between 1089-1039 cm^{-1} are associated to $n3$ vibrations of (PO_4^{3-}) (Komath, Varma *et al.* 2000). The band revealed around 1459 cm^{-1} ($v3$) evidences the presence of small amount of CO_3 in the sample. This band corresponds to CO_3^{2-}, which indicates the formation of carbonate apatite (Tampieri, Celotti *et al.* 1997). The presence of 1459 cm^{-1} ($v3$) band may be due to the atmospheric CO_2 as no carbon-containing precursor was used for our HAp synthesis. The IR absorption bands appeared around 3573 and 632 cm^{-1} for the biomaterial are the stretching and vibrational modes, respectively, of OH^- ions (Furuzono, Sonoda *et al.* 2001).

3.3 BET analysis

N_2 adsorption-desorption isotherm at 77K (Fig. 3(a)) was used for texture analysis of the synthesized HAp nanoparticles. The isotherm revealed the characteristics of type IV mesoporous materials (UPAC classification) with hysteresis associated to the capillary condensation in the solid (Fu, Ho *et al*. 2008). The calcinated HAp sample exhibits a hysteresis loop with sharp adsorption at P/Po > 0.8 indicating its high surface area. The BET analysed average surface area of the nanostructures was estimated to be of 78.415 m^2g^{-1}. Average pore size and pore volume of the sample were estimated to be 24.468 nm and 0.4797 cc g^{-1}, respectively.

3.4 TG-DTA analysis

TG-DTA analysis measures the weight loss of a sample with respect to temperature and hence its thermal stability and phase transition, if any. In the TG-DTA curves presented in Fig. 3(b), we can observe three major mass loss stages for the sample. The first major weight loss can be noted in-between 60-180°C, the second weight loss between 275 and 280°C, and the third in 390-440°C range on heating the sample from room temperature to 1200°C (Mondal, Mondal *et al*. 2012). The estimated first, second and third major weight losses were ~5.56%, ~6.5% and ~5.2% of the sample taken for experimentation, respectively. The first mass loss might be due to the removal of adsorbed water from sample surface and inter-particle spaces (Mondal, Mondal *et al*. 2012, 2014).
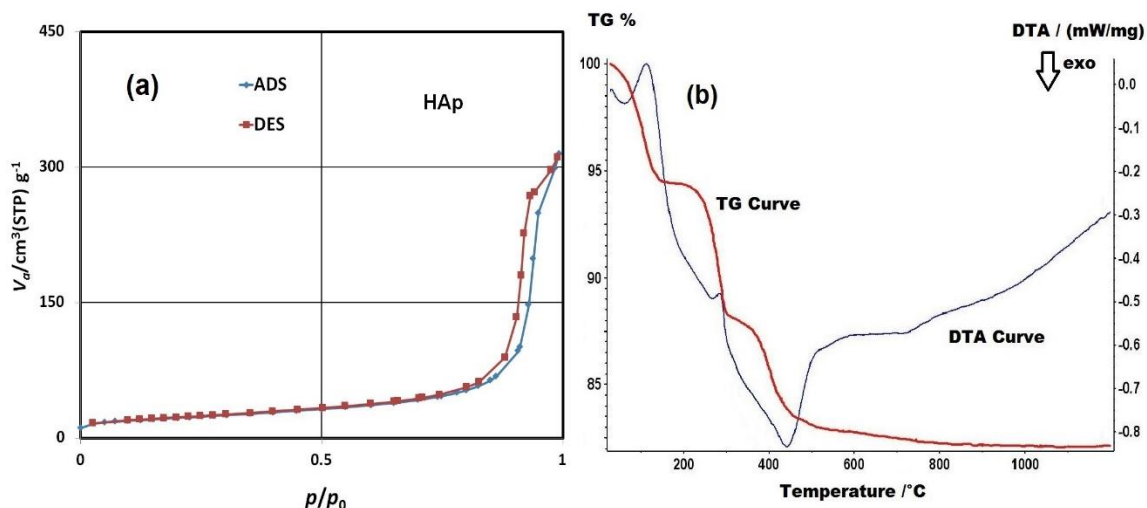
Fig. 3 (a) N_2 adsorption-desorption isotherm and (b) TG-DTA curves of the calcinated HAp nanoparticles

Three major exothermic peaks observed at ~89.4°C, ~270°C and ~430°C for the HAp sample. The first exothermic peak basically corresponds to the loss of residual (adsorbed and hydrated) water. The second exothermic peak appeared at ~270°C is attributed to the dehydration of intracrystalline water, which causes partial formation of oxyhydroxyapatite (Khal and Batis 2015). The chemical reaction associated to this process can be expressed as

$$Ca_{10}(PO_4)_6(OH)_2 \rightarrow Ca_{10}(PO_4)_6(OH)_{2-2y}O_y + yH_2O \tag{2}$$
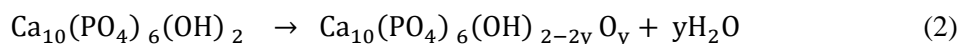
The third exothermic peak appeared at ~430°C corresponds to the decomposition of carbonate ions which endorses the release of CO_2 (Khal and Batis 2015). The reaction associated to the process can be written as

$$Ca_{10-x}(PO_4)_{6-x}(CO_3)_x(OH)_2 + \left(\frac{x}{3}\right)H_2O \leftrightarrow \left(\frac{1-x}{6}\right)Ca_{10}(PO_4)_6(OH)_2 + \left(\frac{2x}{3}\right)CaO + xCO_2 \tag{3}$$
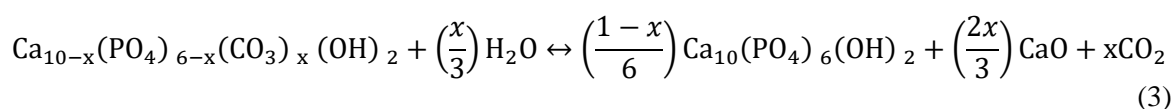
The three major endothermic peaks recorded at ~142.7°C, ~298°C, ~415°C for the HAp sample might be associated to the evaporation of free water, along with the decomposition of ammonium nitrate (NH_4NO_3), which is the residual product of HAp synthesis (Eq. (1)). The endothermic peak appeared at ~415°C has also been attributed to the loss of structural water from HAp by Song, We *et al*. (2002), Biamino and Badini (2004). Therefore, the observed total weight loss (~17.26%) can be associated to water evaporation, and combustion of inorganic byproducts from HAp sample. However, the weight loss observed for the synthesized HAp nanostructures in-between 650 and 1200°C was minimum (~0.8%), indicating their high thermal stability up to 1200°C.

3.5 Thermal stability of HAp nanoparticles

It is generally accepted that heating of HAp leads to three concurrent processes, which involve: i) the evaporation of water, ii) dehydroxylation, and iii) decomposition. Although there is an

Table 2 Thermal effects on hydroxyapatite

Temperature	Reactions
25-200℃	Evaporation of absorbed water
200-600℃	Evaporation of lattice water
600-800℃	Decarbonation
800-900℃	Dehydroxylation of HAp forming partially or completely decarboxylated oxyhydroxyapatite (OHAp)
1050-1400℃	HAp decomposes to form β TCP and TTCP
<1120℃	Stable β TCP
1120℃-1470℃	β TCP is converted to α TCP
1550℃	Melting temperature of HAp
1630℃	Melting temperature of TTCP, leaving behind CaO
1730℃	Melting temperature of TCP
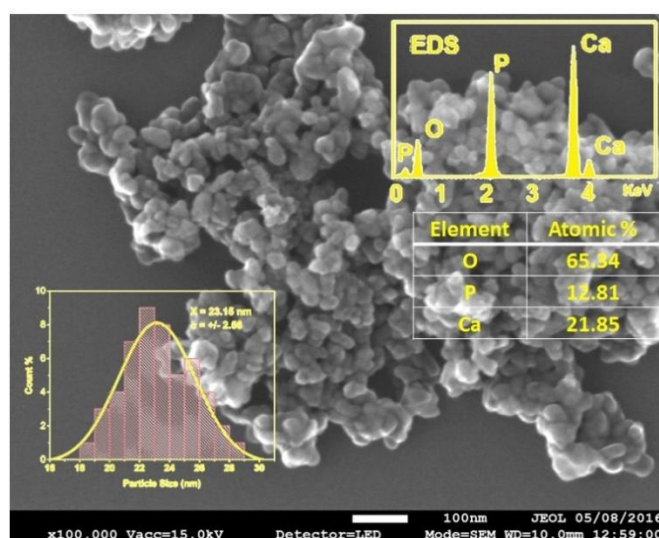
Fig. 4 Typical SEM image and EDS spectrum of the calcinated HAp nanoparticles

agreement between researchers about the processes, which occur during thermal treatment of HAp, it is difficult to predict the exact temperatures at which these reactions occur. This is because the reactions do not occur instantly but over a wide temperature range, which depends on a number of factors associated to both the environment and the composition of the HAp.

The highest thermal stability which has been found in the literature is reported by Deram, Minichiello *et al*. (2003), where HAp powder samples didńt show any phase transformation up to a temperature of 1450℃. The decomposition of HAp into, β- TCP (β-Tricalcium phosphate), TTCP (Tetracalcium phosphate) and α-TCP (α-Tricalcium phosphate), has been reported to begin at 1050℃ by Sridhar, Mudali *et al*. (2003) and at 1200℃ by Tampieri, Celotti *et al*. (2000). A melting temperature of 1550℃ was reported for phase pure HAp; 1630℃ for TTCP and 1730℃ for TCP (Lowell 1979). The temperature ranges in which the reactions occur on heating HAp from ambient temperature to 1730℃ are summarized in Table 2 (Lowell 1979).
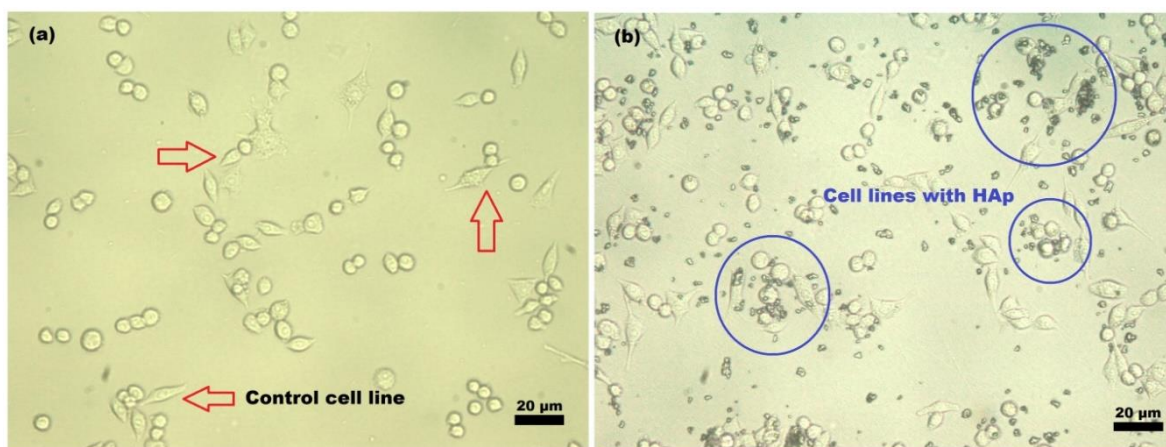
Fig. 5 Trypan blue in vitro cell viability study of synthesized HAp powder
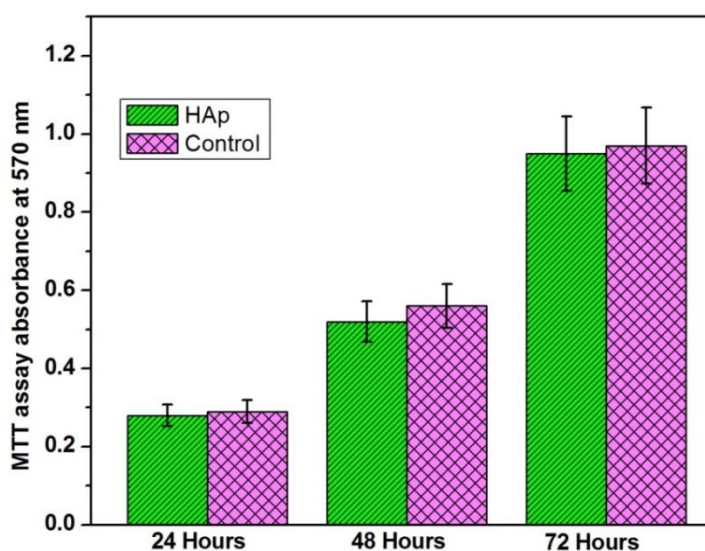
Fig. 6 Biological in vitro evaluation (MTT assay) of synthesized HAp nanoparticles

3.6 SEM and EDS analysis

The SEM study reveals the formation of well-dispersed spherical HAp nanoparticles in the sample (Fig. 4). The HAp particles are nearly spherical and have average diameter of 23.15 ± 2.56 nm. The EDS analysis revealed the presence of Ca, P, and O in the sample with Ca/P ratio of 1.70.

3.7 Biocompatibility and toxicity tests

The experimental result for Trypan blue assay reveals that, approximately all the test cells are living and healthy in presence of synthesized HAp nano particles. The control cell culture well shows maximum cell proliferation, almost similar with HAp nano particles containing culture

well. The observed cells were healthy and well attached on the culture plate surface as depicted in Fig. 5.

3.8 MTT assay

The MTT assay results suggest that our HAp particles have no toxic effect on the growth of MG63 cells in comparison to the control (Fig. 6). HAp nanoparticle containing culture wells show almost similar viability as that of control cell lines. The study was performed up to 72 h and spectrometric study was performed after each 24 h interval. In day 1, the control cell line showed maximum proliferation of cells. Synthesized HAp shows almost similar viability but a little less than the control one. This might have occurred as HAp particles occupied the culture well space and obstacle the proliferation of new cells.

4. Conclusions

In summary, we could fabricate well dispersed, stoichiometric (Ca/P=1.67) HAp nanoparticles of spherical morphology with average diameter of 23.15±2.56 nm using wet chemical precipitation method. The used method is very simple, which can synthesize HAp nanoparticles in large quantity with high reproducibility. The advantage of this method is its byproducts are soluble in water, and hence the precipitate can be easily washed to recover high purity nano-hydroxyapatite. TG-DTA study revealed a high thermal stability of HAp powder up to 1200℃ in controlled atmosphere. Synthesized HAp sample is porous, with average surface area of 78.415 m^2 g^{-1} and an average pore size and pore volume of 24.468 nm and 0.4797 cc g^{-1}, respectively. Cytotoxicity analysis and MTT assay of the HAp nanoparticles indicate no cytotoxic effects on MG63 osteogenic cell line media. The high bioactivity and nontoxicity of the synthesized water dispersible HAp nanoparticles envisage its potential for medicinal and therapeutic applications.

Conflict of interests

The authors declared no conflict of interests with respect to the research, authorship and publication of this paper.

Acknowledgements

References

Adhikary, K., Takahashi, M. and Kikkawa, S. (2004), "Synthesis and sintering of nanocrystalline

hydroxyapatite powders by citric acid sol-gel combustion method", *Mater. Res. Bull.*, **39**, 25-32.

Biamino, S. and Badini, C. (2004), "Combustion synthesis of lanthanum chromite starting from water solutions: Investigation of process mechanism by DTA-TGA-MS", *J. Eur. Ceram. Soc.*, **24**, 3021-3034.

Deram, V., Minichiello, R., Maguer, A. Le., Pawlowski, L. and Murano, D. (2003), "Microstructural characterizations of plasma sprayed hydroxyapatite coatings", *Surf. Coat. Technol.*, **166**(2003), 153-159.

Fu, Y.C., Ho, M.L., Wu, S.C., Hsieh, H.S. and Wang, C.K. (2008), "Porous bioceramic bead prepared by calcium phosphate with sodium alginate gel and PE powder", *Mater. Sci. Eng. C.*, **28**, 1149-1158.

Furuzono, T., Sonoda, K. and Tanaka, J. (2001), "A hydroxyapatite coating covalently linked onto a silicone implant material", *J. Biomed. Mater. Res.,* **56**(1), 9-16.

Gross, K.A., Berndt, C.C., Stephens, P. and Dinnebier, R. (1998), "Oxyapatite in hydroxyapatite coatings", *J. Mater. Sci.*, **33**(15), 3985-3991.

Han, Y., Wang, X. and Cheni, X. (2004), "Synthesis and sintering of nanocrystalline hydroxyapatite powders by citric acid sol-gel combustion method", *Mater. Res. Bull.*, **39**(1), 25-32.

Jillavenkatesa, A., Hoelzer, D.T. and Condrate, Sr. R.A. (1999), "An electron microscopy study of the formation of hydroxyapatite through sol-gel processing", *J. Mater. Sci.*, **34**(19), 4821-4830.

Kehoe, S. (2008), "Optimisation of hydroxyapatite (HAp) for orthoapedic application via the chemical precipitation technique", PhD Thesis, Dublin City University.

Kehoe, S. (2008), *Calcium Phosphates for Medical Applications*, Eds. L. Looney & J. Stokes, © Dublin City University, ISBN1-87232-776-1, ISSN 1649-8232.

Khal, E.M. and Batis, N.H. (2015), "Effects of temperature on the preparation and characteristics of hydroxyapatite and its adsorptive properties toward lead", *New J. Chem.*, **39**, 3597-3607.

Komath, M., Varma, H.K. and Sivakumar, R. (2000), "On the development of an apatitic calcium phosphate bone cement", *Bul. Mater. Sci.*, **23**(2), 135-140.

Kuriakose, T.A., Kalkura, S.N., Palanichamy, M., Arivuoli, D., Dierks, K., Bocelli, G. and Betzel, C. (2004), "Synthesis of stoichiometric nano crystalline hydroxyapatite by ethanol-based sol-gel technique at low temperature", *J. Cryst. Growth*, **263**, 517-523.

Liu, D.M., Troczynski, T. and Tseng, W.J. (2001), "Water-based sol-gel synthesis of hydroxyapatite: process development", *Biomater.*, **22**(13), 1721-1730.

Liu, D.M., Yang, Q., Troczynski, T. and Tseng, W.J. (2002), "Structural evolution of sol-gel-derived hydroxyapatite", *Biomater.*, **23**(7), 1679-1687.

Lowell, S. (1979), *Introduction to Powder Surface Area*, John Wiley and Sons, Toronto.

Mobasherpour, I., Soulati Heshajin, M., Kazemzadeh, A. and Zakeri M. (2007), "Synthesis of nanocrystalline hydroxyapatite by using precipitation method", *J. Alloy. Compd.*, **430**, 330-333.

Mondal, S., Bardhan. R., Mondal, B., Dey, A., Mukhopadhyay, S.S., Roy, S., Guha, R. and Roy, K. (2012), "Synthesis, characterization and in vitro cytotoxicity assessment of hydroxyapatite from different bioresources for tissue engineering application", *Bull. Mater. Sci.*, **35**(4), 683-691.

Mondal, S., Mahata, S., Kundu, S. and Mondal, B. (2010), "Processing of natural resourced hydroxyapatite ceramics from fish scale", *Adv. Appl. Ceram.*, **109**(4), 234-239.

Mondal, S., Mondal, A., Mandal, N., Mondal, B., Mukhopadhyay, S.S., Dey, A. and Singh, S. (2014), "Physico-chemical characterization and biological response of *Labeo rohita* derived hydroxyapatite scaffold", *Bioprocess. Biosyst. Eng.*, **37**, 1233-1240.

Mondal, S., Mondal, B., Dey, A. and Mukhopadhyay, S.S. (2012), "Studies on processing and characterization of hydroxyapatite biomaterials from different bio wastes", *J. Miner. Mat. Charac. Eng.*, **11**(1), 55-67.

Mondal, S., Pal, U. and Dey, A. (2016), "Natural origin hydroxyapatite scaffold as potential bone tissue engineering substitute", *Ceram. Int.*, dx.doi.org/10.1016/j.ceramint.2016.08.165.

Monma, H. and Takahashi, T. (1987), "Preparation and thermal changes of carbonate containing apatite", *Gypsum and Lime.*, **210**, 287-291.

Morales, J.G., Burgues, J.J., Boix, T., Fraile, J. and Clemente R.R. (2001), "Precipitation of stoichiometric hydroxyapatite by a continuous method", *Cryst. Res. Technol.*, **36**(1), 15-26.

Nagai, M. and Nishino, T. (1988), "A new type of CO_2 gas sensor comprising porous hydroxyapatite

ceramics", *Sensor. Actuat.*, **15**(2), 145-151.

Nasiri-Tabrizi, B., Honarmandi, P., Ebrahimi-Kahrizsangi, R. and Honarmandi, P. (2009), "Synthesis of nanosize single-crystal hydroxyapatite via mechanochemical method", *Mater. Letts*., **63**, 543-546.

Panda, R.N., Ming-Fa, H., Chung, R.J. and Chin, T.S. (2001), "X-Ray diffractometry and X-Ray photoelectron spectroscopy investigations of nanocrytalline hydroxyapatite synthesized by a hydroxide gel technique", *Jpn. J. Appl. Phys*., **40**, 5030-5035.

Raynaud, S., Champion, E., Assollant, D.B. and Thomas, P. (2002), "Calcium phosphate apatites with variable Ca/P atomic ratio I. Synthesis, characterisation and thermal stability of powder", *Biomater.*, **23**(4), 1065-1072.

Rivera, E.M., Araiza, M., Brostow, W., Castano, V.M., Diaz-Estrada, J.R., Hernandez, R. and Rodriguez., J.R. (1999), "Synthesis of hydroxyapatite from eggshells", *Mater. Lett*., **41**(3), 128-134.

Sarig, S. and Kahana, E. (2002), "Rapid formation of nanocrystalline apatite", *J. Crystal Growth*., **237**, 55-59.

Shih, W.J., Chen, Y.F., Wang, M.C. and Hon, M.H. (2004), "Crystal growth and morphology of the nano-sized hydroxyapatite powders synthesized from $CaHPO_4 \cdot 2H_2O$ and $CaCO_3$ by hydrolysis method", *J. Cryst. Growth*, **270**, 211-218.

Shojai, M.S., Khorasani, M.T., Khoshdargi, E.D. and Jamshidi. A. (2013), "Synthesis methods for nanosized hydroxyapatite with diverse structures", *Acta Biomater.*, **9**(8), 7591-7621.

Song, T., Wen, S. and Li, M. (2002), "The investigation on preparation and physicochemical process of nanosized hydroxyapatite powder", *Mat. Res. Soc. Symp. Proc*., **724,** 135-140.

Sridhar, T.M., Mudali, U.K. and, Subbaiyan, M. (2003), "Sintering atmosphere and temperature effects on hydroxyapatite coated type 316L stainless steel", *Corros. Sci*., **45**(10), 2337-2359.

Stockert, J.C., Castro, A.B., Cañete, M., Horobin, R.W. and Villanueva, A. (2012), "MTT assay for cell viability: Intracellular localization of the formazan product is in lipid droplets", *Acta Histochemica.*, **114**(8), 785-796.

Tampieri, A., Celotti, G., Sprio, S. and Mingazzini, C. (2000), "Characteristics of synthetic hydroxyapatites and attempts to improve their thermal stability", *Mater. Chem. Phys.*, **64**(1), 54-61.

Tampieri, A., Celotti, G., Szontagh, F. and Landi, E. (1997), "Sintering and characterization of HA and TCP bioceramics with control of their strength and phase purity", *J. Mater. Sci. Mater. Med*., **8**(1), 29-37.

Tanaka, H., Chikazawa, M., Kandori, K. and Ishikawa, T. (2000), "Influence of thermal treatment on the structure of calcium hydroxyapatite", *Phys. Chem. Chem. Phys.*, **2**, 2647-2650.

Tsui, Y.C., Doyle, C. and Clyne, T.W. (1998), "Plasma sprayed hydroxyapatite coatings on titanium substrates Part 1: Mechanical properties and residual stress levels", *Biomater.*, **19**(22), 2015-2029.

Uskokovi´c, V. and Wu, M.V. (2016), "Calcium Phosphate as a Key Material for Socially Responsible Tissue Engineering", *Mater.*, **9**(434), 1-27.

Vaidhynathan, B. and Rao, K.J., (1996), "Rapid microwave assisted synthesis of hydroxyapatite", *Bull. Mater. Sci*., **19**(6) 1163-1165.

Varma, H.K., Kalkura, S.N. and Sivakumar, R. (1998), "Polymeric precursor route for the preparation of calcium phosphate compounds", *Ceram. Int*., **24**(6), 467-470.

Xu, J.L., Khor, K.A., Dong, Z.L., Gu, Y.W., Kumar, R. and Cheang, P. (2004), "Preparation and characterization of nano-sized hydroxyapatite powders produced in a radio frequency (RF) thermal plasma", *Mater. Sci. Eng. A*., **374**, 101-108.

JL